Science Bulletin xxx (xxxx) xxx

Contents lists available at ScienceDirect

Science Bulletin

journal homepage: www.elsevier.com/locate/scib

Article

Non-equilibrium compression achieving high sensitivity and linearity for iontronic pressure sensors

Jing Yang [a,1], Zhibin Li [a,1], Ying Wu [b,1], Yong Shen [a], Ming Zhang [c], Bin Chen [d], Guojiang Yuan [a], Songhua Xiao [a], Jiansong Feng [a], Xu Zhang [a], Yuwei Tang [a], Sunan Ding [e,*], Xiaolong Chen [a,*], Taihong Wang [a,b,*]

[a] Department of Electrical and Electronic Engineering, Southern University of Science and Technology, Shenzhen 518055, China
[b] School of Microelectronics, Southern University of Science and Technology, Shenzhen 518055, China
[c] Key Laboratory for Micro/Nano Optoelectronic Devices of Ministry of Education, Engineering Research Center of Advanced Semiconductor Technology and Application of Ministry of Education, Changsha Semiconductor Technology and Application Innovation Research Institute, College of Semiconductors (College of Integrated Circuits), Hunan University, Changsha 410082, China
[d] School of Environmental and Chemical Engineering, Yanshan University, Qinhuangdao 066004, China
[e] School of Integrated Circuits, Nanjing University, Suzhou 215163, China

ARTICLE INFO

Article history:
Received 8 October 2023
Received in revised form 2 April 2024
Accepted 8 May 2024
Available online xxxx

Keywords:
Artificial mechanoreceptor
Pressure sensor
Vertical grapheme
Ionic nanofiber
Object recognition
E-skin

ABSTRACT

Flexible pressure sensors with high sensitivity and linearity are highly desirable for robot sensing and human physiological signal detection. However, the current strategies for stabilizing axial microstructures (e.g., micro-pyramids) are mainly susceptible to structural stiffening during compression, thereby limiting the realization of high sensitivity and linearity. Here, we report a bending-induced non-equilibrium compression process that effectively enhances the compressibility of microstructures, thereby crucially improving the efficiency of interfacial area growth of electric double layer (EDL). Based on this principle, we fabricate an iontronic flexible pressure sensor with vertical graphene (VG) array electrodes. Ultra-high sensitivity (185.09 kPa^{-1}) and linearity (R^2 = 0.9999) are realized over a wide pressure range (0.49 Pa–66.67 kPa). It also exhibits remarkable mechanical stability during compression and bending. The sensor is successfully employed in a robotic gripping task to recognize the targets of different materials and shapes based on a multilayer perception (MLP) neural network. It opens the door to realizing haptic sensing capabilities for robotic hands and prosthetic limbs.

1. Introduction

Flexible pressure sensor, also known as electronic skin, exhibits skin-like properties. Its ability to convert external mechanical stimuli into electrical signals makes it an important medium for interaction between humans, robots, and the external environment [1–3]. Sensitivity and linearity are important parameters for evaluating the performance of pressure sensors [4–7]. High sensitivity facilitates the precise sensing of external mechanical stimuli. High linearity can effectively simplify the data processing circuit and obviate the need for multiple calibration processes, thus improving the overall response speed of the sensing system [8]. A capacitive tactile sensor comprises a soft medium sandwiched between two electrodes, converting external mechanical stimuli into capacitive signals. Over recent decades, capacitive tactile sensors have received considerable attention from researchers owing to their simple structure and minimal signal drift [9,10]. Traditional capacitive sensors mainly use rubber as the dielectric layer, which has a limited compression range (soft dielectric volume is constant when compressed), thus, the sensors tend to exhibit low sensitivity. In recent years, the sensitivity of capacitive sensors has been improved by introducing ionic gels [11,12], hydrogels [13,14] or other dielectric layers with free ions [15] to form nanoscale ion–electron interfaces with ultra-high specific capacitance. In this type of iontronic pressure sensors, the variation in the contact area between the electrode and ionic active layer under applied pressure is the key to generating the sensing signal [16]. The introduction of specially designed microstructures on the electrode or

* Corresponding authors.
E-mail address: wangth@sustech.edu.cn (T. Wang).
[1] These authors contributed equally to this work.

https://doi.org/10.1016/j.scib.2024.05.001

Please cite this article as: J. Yang, Z. Li, Y. Wu et al., Non-equilibrium compression achieving high sensitivity and linearity for iontronic pressure sensors, Science Bulletin, https://doi.org/10.1016/j.scib.2024.05.001

dielectric surface can effectively expand the range of variation of the electric double layer (EDL) area, thus improving the sensitivity and pressure response range of the sensors. However, current major microstructural strategies, such as pyramids [12] and microdomes [17], exhibit stable axisymmetric structures that depend primarily on axial compression deformation. The increase in structural stiffness during compression improves its compressive strength, making it difficult to flatten the microstructure further. Thus, the realization of high sensitivity and linearity is fundamentally limited [18]. The lateral deformation that follows axial equilibrium compression instability in microcolumns with high aspect ratios softens the stiffness and enhances sensitivity [19]. But this equilibrium destabilization process requires a certain amount of axial compression accumulation before it occurs, and it does not improve the sensitivity at the beginning of the compression process. How to significantly improve the growth efficiency of the EDL interface area is crucial for constructing a highly sensitive iontronic pressure sensor.

Here, we present an iontronic pressure sensor using vertical graphene (VG) array electrodes. It features an inclined branching flap-like microstructure designed to circumvent the initial axial compression process. The non-equilibrium compression resulting from lateral bending deformation confers superior compressibility to the VG array, which plays a crucial role in increasing the contact area between the electrode and active layer. The VG-based pressure sensor demonstrates ultra-high sensitivity (185.09 kPa^{-1}) and high linearity (R^2 = 0.9999) within a pressure range of 0.49 P a–66.67 kPa. Furthermore, it exhibits excellent mechanical stability, enduring over 1000 compressions/releases at 5 kPa or 1000 bends/releases at a bending radius of 4 mm without significant fatigue. In addition, it maintains a tiny pressure resolution of 25 Pa at a preload pressure of 10 kPa. We construct a 4 × 4 sensor array with real-time signal acquisition for the robotic hand to precisely identify objects. The total classification accuracy in recognizing the eight types of objects reaches 89.1%, indicating the feasibility of using a robotic hand armed with a tactile sensing array for object recognition.

2. Materials and methods

2.1. Materials

Thermoplastic polyurethane (TPU-1065A) was purchased from DaDong Resin Chemical Co., Ltd. Poly (vinylidene fluoride-co-hexa fluoropropylene) (PVDF-HFP) was purchased form Sigma-Aldrich. 1-Butyl-3-methylImidazolium bis(trifluoromethylsulfonyl)imide ([BMIM][TFSI]) was purchased from Langang Greenchem. *N,N*-dimethylformamide (DMF, reagent pure) was purchased form Shanghai Macklin Biochemical Technology Co., Ltd. Acetone (Chromatographic reagent) was purchased form Siron Technology Co., Ltd. Polydimethylsiloxane (PDMS, Dow Corning dc184) was purchased from Dow Chemical. Carbon paste (JW-001) was purchased from Deliou. Co., Ltd.

2.2. Preparation

2.2.1. Preparation of flexible VG array

The VG thin-film materials were provided by Yick Xin Technology Development Ltd. Co. (Shenzhen, China). Firstly, the flexible graphene substrate was ultrasonically cleaned with acetone and ethanol, and then dried in air. The dried substrate was placed on a resistively heated sample bench in a radio frequency-plasma enhanced chemical vapor deposition (RF-PECVD). The temperature of the substrate was controlled between 600 and 900 °C using thermocouples. During the deposition, the RF power was maintained at 1000–2000 W. The mass flow rate and pressure of the total gas were controlled at 5–10 mL/min (standard cubic centimeters per minute) and 6–12 Pa, respectively. Methane was chosen as the carbon source and the volume concentration in the H_2 atmosphere was 5%–100%. The deposition time was in the range of 5–40 min.

2.2.2. Preparation of flexible ionic nanofiber active layer

The active layer of the VG sensors was fabricated using our previously reported methods [20]. Firstly, 18 wt% TPU was added to a solvent mixture of DMF and acetone in a mass ratio of 3:2. The shell layer precursor solution was obtained after TPU was completely dissolved. Then, 10 wt% PVDF-HFP was added to the solvent mixture in the same proportion as above, while [BMIM][TFSI] with a mass of 1.5 times the mass of PVDF-HFP was added. A homogeneous core layer precursor solution was obtained. During electrostatic spinning, the propulsion rates of the shell precursor solution and core precursor solution were 0.3 and 0.15 mL/h, respectively. A continuously rotating aluminum roller located 10 cm directly in front of the needle was used to collect nanofibers. A high voltage of 18 kV was applied between the coaxial needle (the inner diameter of the outer needle was 1.12 mm and the inner needle was 0.37 mm) and the aluminum drum. The ambient temperature was maintained at 30 °C.

2.2.3. Preparation of sandpaper electrode and carbon paste electrode

The PDMS and the curing agent were mixed at a 10:1 wt ratio and spin-coated onto sandpaper at 500 r/min for 60 s. After curing at 80 °C for 2 h, PDMS was peeled off from the sandpaper. Ag (100 nm) was deposited on the surface of PDMS microstructures by magnetron sputtering and cut to the desired size as sandpaper electrodes. The conductive carbon paste was printed on a polyethylene terephthalate (PET) substrate with a thickness of 0.03 mm by screen printing method, and the printed PET film was dried at 80 °C for 6 h. Finally, it was cut to the desired size to obtain the carbon paste electrode.

2.2.4. Fabrication of VG sensor

The VG array was cut into 1 cm × 1 cm square. Conductive cloth was used as the conductive wire, and silver glue was used to bond with the conductive cloth to obtain the VG electrodes. After fixing one VG electrode with polyimide tape, a 1.2 cm × 1.2 cm size nanofiber membrane and another VG electrode were stacked sequentially. It should be noted that both the top and bottom electrodes were selected with the VG side facing the nanofiber membrane. The final top layer was encapsulated with a PDMS membrane with a thickness of 50 μm.

2.2.5. Fabrication of VG sensor array

Firstly, a PET film coated with silver paste was cut into a patterned electrode matching the shape of the robot hand using a laser engraving machine. Then the graphite paper side of the VG electrode was fixed to the sensing site of the patterned electrode by silver paste. Thirdly, the cut ionic nanofiber membrane was sandwiched between two patterned electrode arrays with fixed VG electrodes. Finally, it was encapsulated with polyimide tape and fixed to the robotic hand with a double-sided adhesive.

2.3. Finite element analysis

Finite element analysis was performed using ABAQUS 2020. Based on experimental measurements, the Young's modulus of the VG array was set to 930 MPa and Poisson's ratio was referenced to a literature value of 0.149 [21]. The active layer was simply treated as a rigid plate and compressed downward. All contact interactions were assumed to be frictionless and without penetration.

2.4. Characterization and measurements

The morphology of the VG arrays and nanofiber films were characterized using field-emission scanning electron microscopy (FE-SEM, GeminiSEM 300, ZEISS). Capacitance measurements were taken at a frequency of 100 Hz with a 100 mV AC signal (except as noted in the article) using a Keysight E4980AL Precision LCR Meter. Three different batches of VG sensors were tested for compression-release response over a pressure range of <66.67 kPa to avoid chance errors. External pressure was controlled and recorded using a tensiometer (LD23.501, LSD). For the bending measurement, the force was controlled by a linear electrode (LinMot) with a bending radius of 4 mm. Surface chemical information was characterized by Raman spectroscopy (LabRAM HR 800, HORIBA) and X-ray photoemission spectroscopy (XPS, PHI 5000 Versaprobe II, ULVAC-PHI). The VG cross-section was prepared by focused ion beam (FIB) cutting (FEI Scios DualBeam FIB, Thermo Fisher).

2.5. Construction of the neural network model for object recognition system

Multilayer perception (MLP) network and convolutional neural network (CNN) were constructed in PyTorch framework to implement the cognitive process of the robotic hand system. The MLP model has three hidden layers and introduces ReLU nonlinear elements as activation functions. The SoftMax activation function is used to perform the output. CNN mainly included convolution layer and max pooing layer. For the kernel of the convolution layer, the size and stride were 2×2 and 1, respectively.

2.6. Experiments on human subjects

Informed consent was obtained from each human subject, and all experiments were conducted under approval from the Institutional Review Board at the Southern University of Science and Technology with protocol number of 20210138.

3. Results

3.1. Preparation and characterization of VG pressure sensors

Bottom-up *in situ* grown VGs have a special flap-like branching microstructure, and the graphene sheet is not a completely vertically stable axisymmetric equilibrium structure. The angle between the initial graphene sheet and substrate makes it susceptible to a non-equilibrium compression process of flexural deformation when subjected to an external force. This greatly improves the growth efficiency of the contact area between the VG electrode and ion-active layer. Fig. 1a depicts the schematic diagram of VG sensor. VG arrays grown on flexible graphite paper is used as the top and bottom electrodes. Notably, the bottom electrode is secured in place by polyimide tape. The active layer sandwiched between the two electrodes uses the ionic nanofiber membrane reported in our previous work [20]. Finally, the top of the device is encapsulated by PDMS film. Fig. 1b and the experimental section illustrate the growth process of VG arrays on a flexible graphite paper substrate. The ultrasonically cleaned and dried flexible graphite paper substrate is placed in the RF-PECVD system. Methane gas is used as a carbon source for VG array growth. In the plasma, methane undergoes inelastic collisions with electrons, resulting in dissociation and the formation of free radicals, ions and other reactive substances. The growth of VG starts from the growth of planar graphene, and many researchers have analyzed the growth mechanism of VG, but there is no clear conclusion yet [11]. What is certain, however, is that the electric field plays a crucial role in this process. The literature shows that during the growth process, charges accumulate on the graphene flakes. Consequently, the growth direction of the graphene flakes changes to vertical outward protruding growth under the influence of Coulomb repulsion. In particular, the electric field is stronger at the sharp features on the substrate. Additionally, the diffused carbon atoms along the VG surface also move in the direction of the strong electric field, thus promoting the vertical growth of graphene [22–24]. The graphene nanosheets are driven by the vertical electric field of the plasma sheath to grow, and eventually the surface of the graphite paper substrate is completely covered by this VG array with a special branching sheet-like microstructure in a uniform manner. The interconnecting network between the underlying graphite and VG sheet layers confers high conductivity to the microstructured electrode. Meanwhile, the rich microstructure greatly increases the specific surface area of the electrode, and the gaps between the graphene sheets provide sufficient deformation space for the compression of the VG.

In iontronic pressure sensors, the variation of EDL capacitance is the key to affecting sensitivity. According to the Gouy-Chapman-Stern model, the EDL present extremely high unit area capacitance (UAC). This is because the electrons on the electrode surface and the ionic charge in the active layer can be kept at a very close distance ($\sim$1 nm) by the electric field force of the electrode plate. The capacitance of the EDL can be equivalently simplified using the following equation [16]:

$$C_{EDL} = UAC \cdot A, \tag{1}$$

where A is the contact area between electrode and ionic active layer. When external mechanical stress is applied to the device surface, the change in A will produce a significant response signal. As shown in Fig. 1c, when the device is subjected to external mechanical stress, the VG array is easily bent and deformed under stress. This leads to a rapid increase in the A between the VG electrode and ion-activated membrane. At this time, the response capacitance of the sensor also increases rapidly with the increase of the contact. Thus, the device exhibits excellent stress response sensitivity. Fig. 1d, e show the SEM images of VG at magnification of 10k$\times$ and 50k$\times$ in a 45° tilt view, respectively. The 3D network structure of the branching flap-like VG nanosheets is clearly visible in the figure and is uniformly distributed over the entire graphite paper surface. Fig. 1f shows the SEM image of the VG cross section after FIB cutting. It can be seen that the height of the upright grown graphene sheet layer is $\sim$1.4 μm. And the graphene sheet shows a certain inclination distribution between the graphene sheet and the substrate. Core-shell structured ionic nanofiber membrane is the active layer of VG sensor. The ionic liquid ([BMIM][TFSI]) and PVDF-HFP composite ionic nanofibers are embedded in the TPU matrix by coaxial electrostatic spinning technique. The fabrication process of the ionic nanofiber membrane is shown in Fig. S1 (online), and specific experimental details are provided in the experimental section of the article. Fig. 1g shows high-resolution SEM images of the ionic nanofibers and the response mechanism when subjected to pressure. When subjected to external mechanical stimulation, ions in the core layer are pumped and migrate to the shell layer under the electric field force, forming an EDL at the electrode interface, which causes significant changes in the capacitance of the VG sensor. The mechanistic analysis of ionic nanofibers based on this core–shell structure is demonstrated in detail in our previous work [20]. The core–shell structure of the nanofibers can also reduce the initial capacitance of the device, thus increasing device sensitivity.

As mentioned previously, the compressibility of the microstructure of the sensor interface determines its sensing properties. We further investigated the deformation mechanism of the VG array electrode with inclined flap-like microstructure by finite element

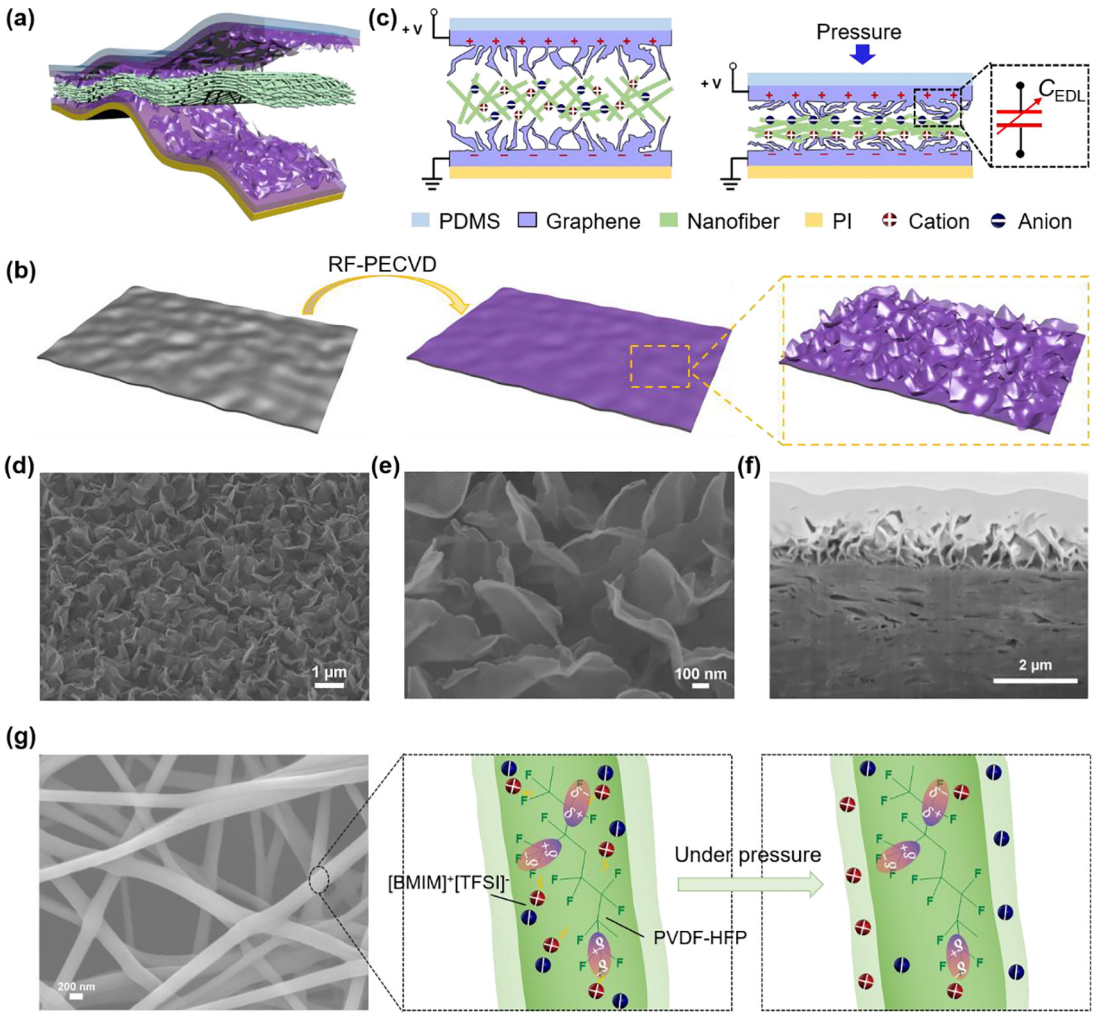

Fig. 1. The structure and sensing mechanism of VG sensor. (a) Schematic illustration of VG sensor. (b) Bottom-upped *in situ* growth of VG on graphite paper substrate. (c) Sensing mechanism of VG arrays-based iontronic sensor. (d, e) 45° tilt-view SEM images of VG electrode at 10k× and 50k× magnification, respectively. (f) SEM image of cross-section of graphite-paper-based VG after FIB cutting. (g) High-magnification SEM image of the ionic nanofibers and the sensing mechanism of core-shell structured ionic nanofibers.

analysis. The simulated schematic diagrams of different compression stages are shown in Fig. 2a. The special microstructure of the VG array can realize a fast bending deformation during the compression process. After the VG electrode forms contact with the active layer, there are still some gaps between the curved lamellar graphene and substrate graphene. These gaps will be gradually filled as the pressure increases, which allows the structure to be further compressed under high pressure. The excellent compressibility of the VG electrodes results in a significant increase of the contact area between the electrode and active layer with the increase of the pressure, which leads to a significant change in the EDL capacitance of the device.

The surface chemical information of VG is characterized by Raman spectroscopy and XPS. In Raman spectrum (Fig. 2b), there are three main distinctive characteristic peaks. The D-band at 1347 cm^{-1} corresponds to the disorder-induced phonon mode, which is attributed to the finite crystallite size effect and various defects induced in sp^2 carbon materials [25]. The G-band peak observed at 1581 cm^{-1}, which is the E_{2g} vibrational mode of sp^2 bonded carbon, indicates the formation of graphitized structure [26]. The intensity ratio of D band to G band (I_D/I_G) is 0.79, showing the existence of abundant edges and defects [27]. This phenomenon matches with the fact that the VG tip exposes a large number of graphene edges. The 2D peak at 2695 cm^{-1} is a second-order vibration caused by the three-dimensional interplanar stacking of the hexagonal carbon networks [26]. The ratio of 2D and G bands ($I_{2D}/I_G \sim 0.84$) indicates that the entire VG array has a large number of multilayer graphene [28]. In addition, the 2D peak shows good symmetry, indicating that the single-layer nature is also present locally in the VG array. The surface chemistry of VG is also analyzed by XPS. A single strong C 1s peak is evident at the binding energy of ~285 eV (shown in Fig. 2c), implying that VG is comprised mostly of carbon atoms. Fig. 2d presents the high-resolution asymmetric C 1s XPS spectrum that can be fitted by four subpeaks corresponding to the C—C bond (sp^2) at the binding energy of ~282.0 eV, sp^3 at the binding energy of ~282.4 eV, carbon—oxygen bond (~283.1 eV), and π–π bond (~287.4 eV), respectively [25,28]. The main reason for the formation of oxygen-containing groups is the presence of reactive dangling bonds in the graphene lattice produced during the CVD process, which are less stable and react rapidly with moisture to form C—O bonds after exposure to air. More importantly, the difference between the C 1s and π–π bond is 6.61 eV, which also proves that the VG array is a mixture of single and multilayer graphene. These characterization results are consistent with the findings reported in the literature [29,30] that the growth process of VG decreases

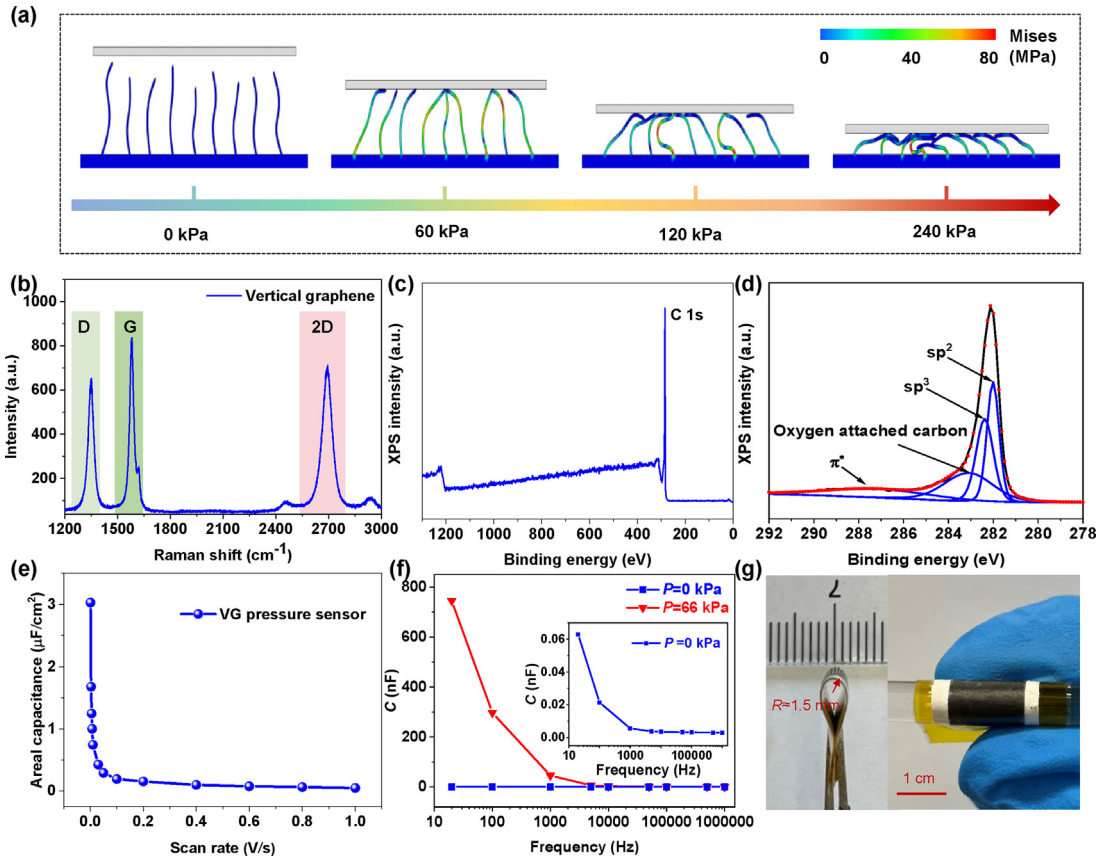

Fig. 2. Finite element analysis and characterization of VG sensor. (a) Simulated stress distribution with ultrathin sheet-like VG structures. (b) Raman spectrum record in the range of 1200–3000 cm^{-1} for VG arrays. (c, d) XPS survey (in the range of 0–1300 eV) and high-resolution C 1s spectrum (in the range of 278–292 eV) of VG arrays, respectively. (e) Effect of different scanning speeds on the capacitance per unit area of VG pressure sensors. (f) Influence of frequency on the initial capacitance (C_0, P = 0 kPa) and the final capacitance (C_P, P = 66 kPa) for VG sensor. (g) Optical picture of VG pressure sensors bent by tweezers (bending radius R≈1.5 mm) and bent on a glass rod.

in number of layers from the bottom up. Thanks to this special bottom-up branching flap-like graphene structure, the electrodes are easily bent and deformed under external stress.

We also performed an electrochemical characterization of the VG sensor using an electrochemical workstation. The cyclic voltammetry (CV) curves of the VG sensor at different scan rates (0.001–1 V/s) are recorded for determining the ion migration characteristics of the EDL. The capacitance per unit area of the sensor at different sweep rates can be calculated from the integrated area of the CV curve, as shown in the following equation:

$$C_A = \frac{1}{2k\Delta VA}\int_{V_1}^{V_2} I(V)\mathrm{d}V \qquad (2)$$

where C_A is the capacitance per unit area, k is the scan rate, V is the voltage window, and A is the area of the sensor. As shown in Fig. 2e, C_A shows a decreasing trend as the scan rate increases. This is due to the limitation of the migration rate of anions and cations at high sweep rates, where the ions do not have sufficient time to generate an EDL according to the polarity of the applied electric field. This phenomenon is also supported by the measurement results of the VG sensor at P = 0 kPa and = 66.67 kPa where the capacitance decreases rapidly with increasing measurement frequency (Fig. 2f). This phenomenon has also been observed in previously reported iontronic pressure sensors. The encapsulated VG sensor has good mechanical flexibility. As shown in Fig. 2g, it can be easily bent to a radius of 1.5 mm.

3.2. Sensing properties of VG sensors

The sensitivity and signal linearity of pressure sensors are key parameters for judging their performance. For capacitive sensors, sensitivity (S) is defined as $S = \delta(C - C_0)/C_0$. C_0 is the initial capacitance in the absence of pressure loading. C is the capacitance when various pressures (P) are applied. Prior to the application of external mechanical stimuli, the device has a low initial capacitance (C_0) thanks to the unique microstructure of the VG array electrodes and the binding of ions by the core–shell structured nanofibers. With the increase of pressure, the inclined-flap VG array was dramatically compressed, the contact area between the electrodes and the ionic nanofiber membrane increased rapidly, while the ions in the core layer were extruded, and the response capacitance increased dramatically with pressure (Fig. S2 online). The blue curve in Fig. 3a shows the normalized change in capacitance of the VG sensor over a pressure range of <66.67 kPa. Over this wide sensing range, the device exhibits ultra-high sensitivity (185.09 kPa^{-1}) and excellent linearity (R^2 = 0.9999). At the same time, the sensitivity performance of different batches of VG devices also shows a good consistency (as shown in Fig. S3 online). In addition, we used the same ionic nanofiber membrane as the dielectric layer, and the performance of the pressure sensors prepared with different electrodes are selected for comparison with that of the VG sensors. As shown in the red curve in Fig. 3a, the device uses PDMS electrodes with a surface excitation of 100 nm Ag with abundant surface microstructure. The electrode used #800 sandpaper as a template, and the microstructure of the electrode surface is shown in Fig. S4 (online).

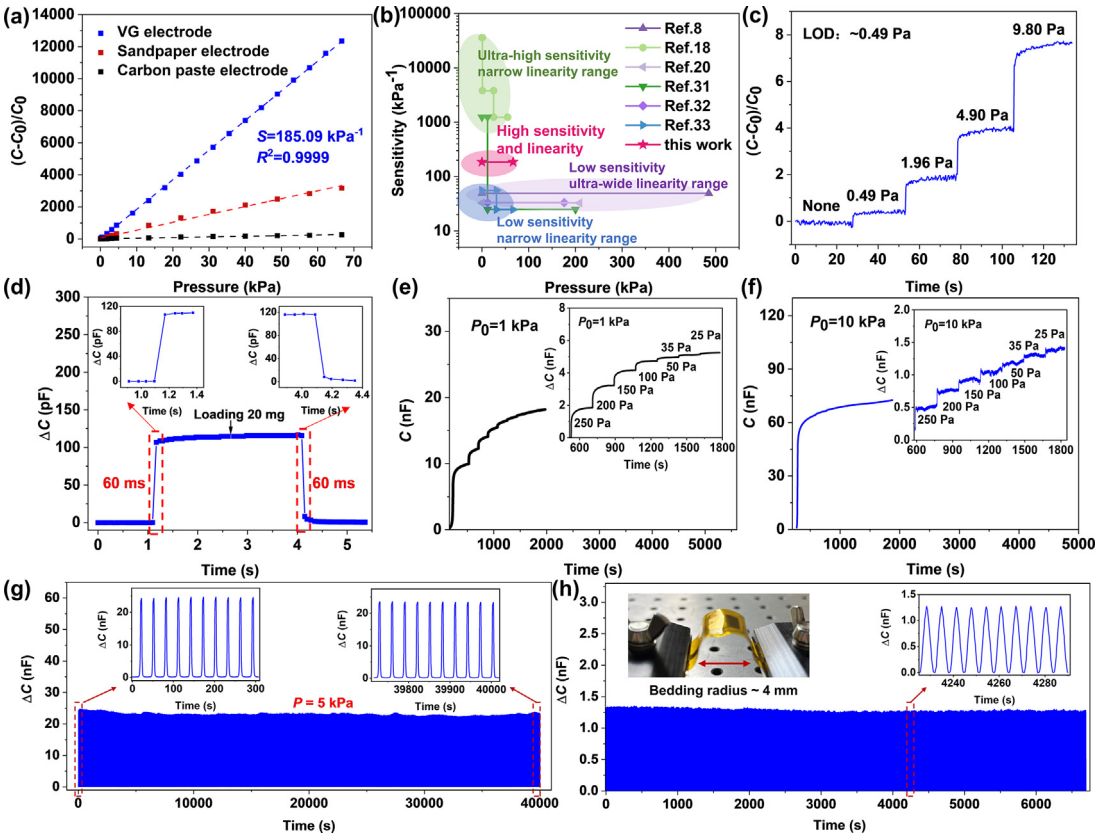

Fig. 3. Sensing properties of the VG sensor. (a) Comparison of the sensitivity of three pressure sensors with the same dielectric layer and different electrodes at static pressure (100 mV@100 Hz). The blue curve shows VG electrodes, the red curve uses PDMS microstructured electrodes with surface sputtered Ag prepared using #800 sandpaper as a template, and the black curve uses PET electrodes coated with carbon paste. (b) Performance comparison of the VG sensor with other recently published capacitive pressure sensors. (c) The surface of the VG sensor is continuously loaded with 0.49, 1.96, 4.90 and 9.80 Pa weights to confirm the ability to detect ultra-low mass target object. (d) The response and recovery time of VG sensor under 20 mg transient pressure stimulus. (e, f) The ability of VG sensor to distinguish micro pressures after preloading with initial pressures of 1 and 10 kPa, respectively. (g) Stability and consistency of the response capacitance during long load/release cycle measurement at 5 kPa. (h) Capacitance signal over 1000 cycles of bending-release at a minimum bending radium (r) of ~4 mm.

The black curve in Fig. 3a uses a PET electrode with direct carbon paste coating. Comparing these two sets of pressure sensors prepared using different electrodes, the VG sensor exhibits extraordinarily high linearity and sensitivity. Although the core–shell structure of ionic nanofibers played a role in enhancing the device performance, the achievement of the final excellent linearity and sensitivity of the device is mainly attributed to the unique microstructure of the VG array electrodes. The performance comparison of the VG sensor with other iontronic pressure sensors [8,18,20,31–33] is shown in Fig. 3b. The comparison of the specific parameters is illustrated in Table S1 (online). High sensitivity and linear response tend to be less compatible in most ionic electronic pressure sensors. The VG pressure sensor exhibits excellent sensitivity and linearity over a pressure range of <66.67 kPa. This provides an advantage for its application to robotic hand recognition.

In addition, VG sensor has good resolution for a range of ultra-small masses and exhibits a low limit of detection (LOD) of 0.49 Pa as evidenced in Fig. 3c. In order to estimate the response and recovery time of the VG sensor after compression, a 20 mg weight is carefully and quickly placed on the top of the device, left for ~3 s and then quickly removed. The response and recovery time of the VG sensor are both 60 ms (as shown in Fig. 3d). Owing to the limitations imposed by the ion migration rate of the dielectric layer and the viscoelasticity of the material, iontronic pressure sensors often require more time to reach equilibrium when subjected to increased external mechanical stimulation. Similarly, after the stimulus is released, they also require a longer time to recover to their initial state. As shown in Fig. S5 (online), the response and recovery times of the VG pressure sensor under compression by a weight of 50 mg are measured to be 93 and 63 ms, respectively. These times are extended to varying degrees compared to the response and recovery times observed under a 20 mg weight stimulus. It is important to note that since the instrument has a higher sampling rate at higher frequencies, a test frequency of 10 kHz is used here to obtain more accurate response and recovery time. The resolution under pressure preload is also an important indicator for selecting pressure sensors. An ideal pressure sensor should be able to detect small pressure changes even when subjected to external pressure in advance. As illustrated in Fig. 3e, f and Fig. S6 (online), the VG sensor has excellent pressure resolution even under three different preloaded pressures of P_0 = 1, 5, and 10 kPa. For the test, the device is first compressed to a specified preload pressure and continued with a small pressure (in the range of 250–25 Pa). The change in the capacitance is measured in real time throughout the process. The results show that small stress increments successfully induce a rapid capacitance response. Our VG sensor can recognize micro-pressures down to 25 Pa at a low-pressure preload of 1 kPa. More importantly, at a high preload of 10 kPa, the device can still successfully distinguish small pressures of 25 Pa with a pressure resolution of 0.25%. For reference, human skin typically has the ability to distinguish a 7% pressure difference at small pressures. Therefore, the VG sensor has the ability to distinguish pressure differences far better than human skin.

For flexible pressure sensors, high mechanical durability during long-term or cyclic use is essential for a reliable signal output. The capacitance normalization curves of the VG sensor under moderate

(0.44, 1.78, 3.11, 4.44 kPa) and high (8.89, 26.67, 44.44, 62.22 kPa) stresses for five compression/release conditions are illustrated in Fig. S7 (online). During this process, the device shows a good stability in line with the applied pressure. To further demonstrate the durability of the device, compression and release measurements are repeated over 1000 cycles at the peak pressure of 5 kPa (Fig. 3g). The insets in Fig. 3g represent the normalized capacitance response curves for the first 10 compression/release cycles and last 10 compression/release cycles, respectively. It can be clearly seen that the device shows no significant signal drift or fluctuation during the compression cycle measurement. The SEM image of the geometric morphology of the VG electrode surface after prolonged cyclic testing is shown in Fig. S8 (online). It can be observed from the figure that the microstructure of the electrode surface remains intact after extended cycles of pressure loading and unloading. This also represents a significant factor that enables VG pressure sensors to achieve excellent mechanical stability. We also conducted a bending cycle measurement to illustrate the flexibility and bending-resistant mechanical durability of the VG sensor based on the stability of the signal during the bending cycle. We conducted more than 1000 bending cycles of bending/straightening with a bending radius of 4 mm, and the capacitance signal is collected in real time during the measurement. The results in Fig. 3h show that the VG sensor has good flexibility and mechanical stability during bending. The left inset in Fig. 3h shows an optical photograph of the device during bending, and the right inset shows the response signal of ten randomly selected tests in the bending/straightening cycle tests. In addition, we individually test the difference between the resistance values of the same VG array electrode in bending or twisting and the initial state (Fig. S9 online). The consistent conductivity of the VG electrode in different mechanical states is also key to ensuring its stability in bending for a long time. The effects of humidity and temperature on sensor performance cannot be ignored either. As shown in Fig. S10 (online), we test the capacitance change of the VG sensor with a 2 g weight placed on the surface in relative humidity environments of 12%, 23%, 43%, 59%, 75%, and 85% and temperature intervals from 20 to 50 °C, respectively. The results show that the capacitance value of VG increases slowly with increasing humidity. The effect of temperature change on the capacitance of the device is more significant. This is mainly influenced by the effect of humidity on the degree of ion dissociation and temperature on the improvement of ion migration kinetic properties. With the increase in humidity and temperature, more ions are involved in the formation of the interfacial EDL, which causes an increase in capacitance.

3.3. Application of the VG sensors in physiological signal monitoring

With continuous socio-economic development, people are becoming more concerned about their health. At the same time, human health has become a hot issue in the field of scientific research. Real-time, *in situ*, long-term monitoring of human movement status and physiological signals plays a crucial role in achieving a more accurate health assessment and early warning of body functions. Especially for many patients with chronic diseases (including Parkinson's, hypertension), long-term

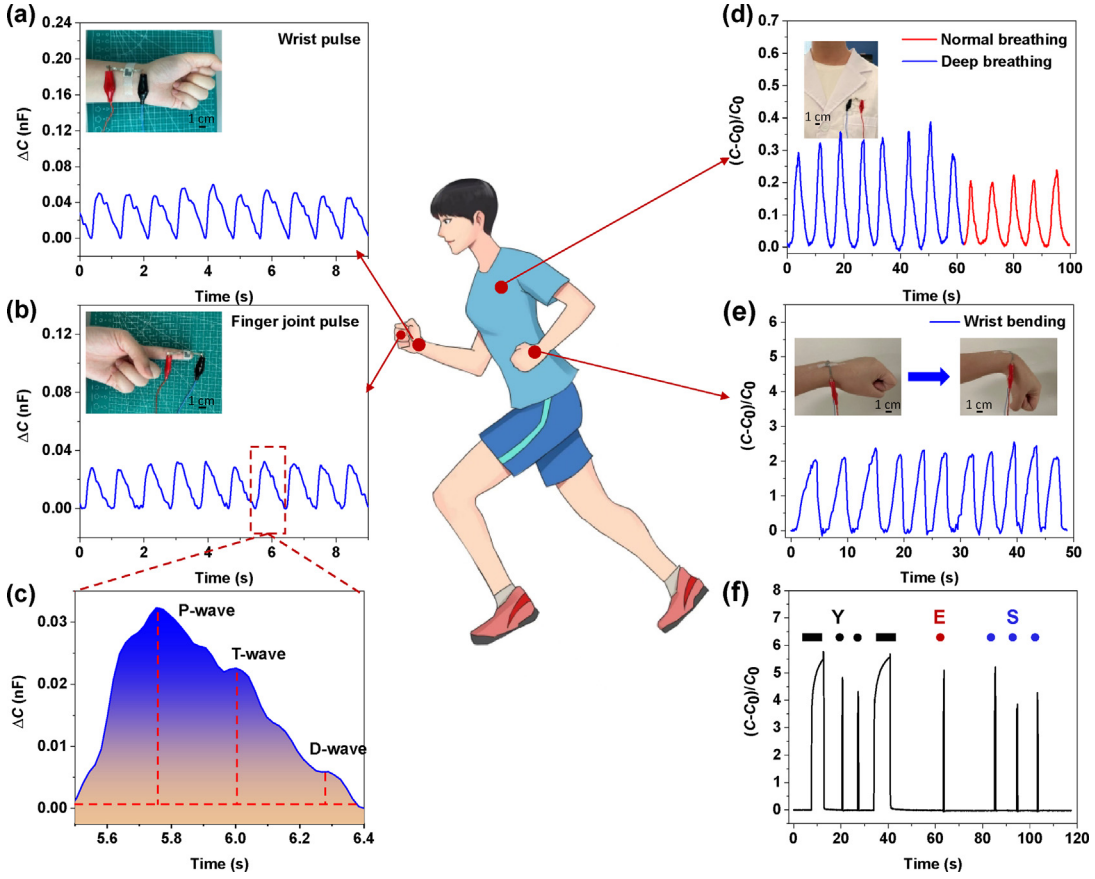

Fig. 4. Application of VG sensors in physiological signal monitoring. (a) Pulse wave signal detected by a VG sensor on the wrist. (b) Pulse wave signal detected by a VG sensor on the fingertip. (c) Typical fingertip pulse wave signal detected by the device. (d) Monitor the capacitance change curve of the device in two modes of normal breathing and deep breathing mode. (e) Capacitance signal change curve captured using VG sensor during wrist bending movement from 0° to 90°. (f) The capacitive response signal of Morse code corresponding to the letter YES is sent by tapping and long press on the device.

real-time physiological monitoring information can improve more comprehensive information for clinicians' diagnosis.

The VG sensor has high sensitivity and linearity, enabling the monitoring of small physiological signals such as pulse and respiration. At the same time, the device is thin, light and flexible. It can be attached to the human skin at different locations without the burden of monitoring signals such as joint flexion and human movement behavior. As shown in Fig. 4a, b, the VG sensors are fixed by medical tape to the wrist and fingertip positions of a volunteer, respectively. It can precisely capture the pulse wave signal at the corresponding positions. Fig. 4c extracts the periodic signal of a continuously monitored fingertip pulse wave. From the figure, the three typical main waves of the pulse wave can be clearly distinguished: P-wave, T-wave and D-wave. Pulse waves are an important component of physiological signals and provide a basis for the diagnosis of cardiovascular diseases and analysis of physical conditions. By attaching the VG sensor to the outer surface of the garment near the chest cavity, the breathing of the body can be monitored in real time by the expansion and undulation of the chest cavity during breathing. As shown in Fig. 4d, the difference in the capacitance signal of the VG sensor can clearly distinguish the two different states of deep breathing and normal breathing. Due to the excellent flexibility of the VG sensor, the response signal has good stability over more than 1000 bending/recovery cycles. The VG sensor is fixed to the volunteer's wrist using medical tape, and the device could accurately output to the change in capacitance signal during wrist bending from 0° to 90° (Fig. 4e). Based on the fast signal response and recovery of the VG sensor after stress, it can also be used for signal transmission of Morse code. Fig. S11 (online) illustrates the Morse code corresponding to the different English characters. We tapped the English word "Yes" on the surface of the device with the finger, and the corresponding capacitive signal is generated for Morse code decoding and signaling (as shown in Fig. 4f). Thanks to its superior electrical and mechanical properties, the VG sensor shows great potential for real-time monitoring of human physiological signals and limb movements. This also provides more possibilities for the development of human–computer interaction and intelligent medicine.

3.4. Object recognition system for robots based on VG sensor array

Humans can recognize object of different shapes and materials using pressure sensors on the skin. Based on this, we develop a robotic hand with an integrated 4 × 4 VG sensor array. As shown

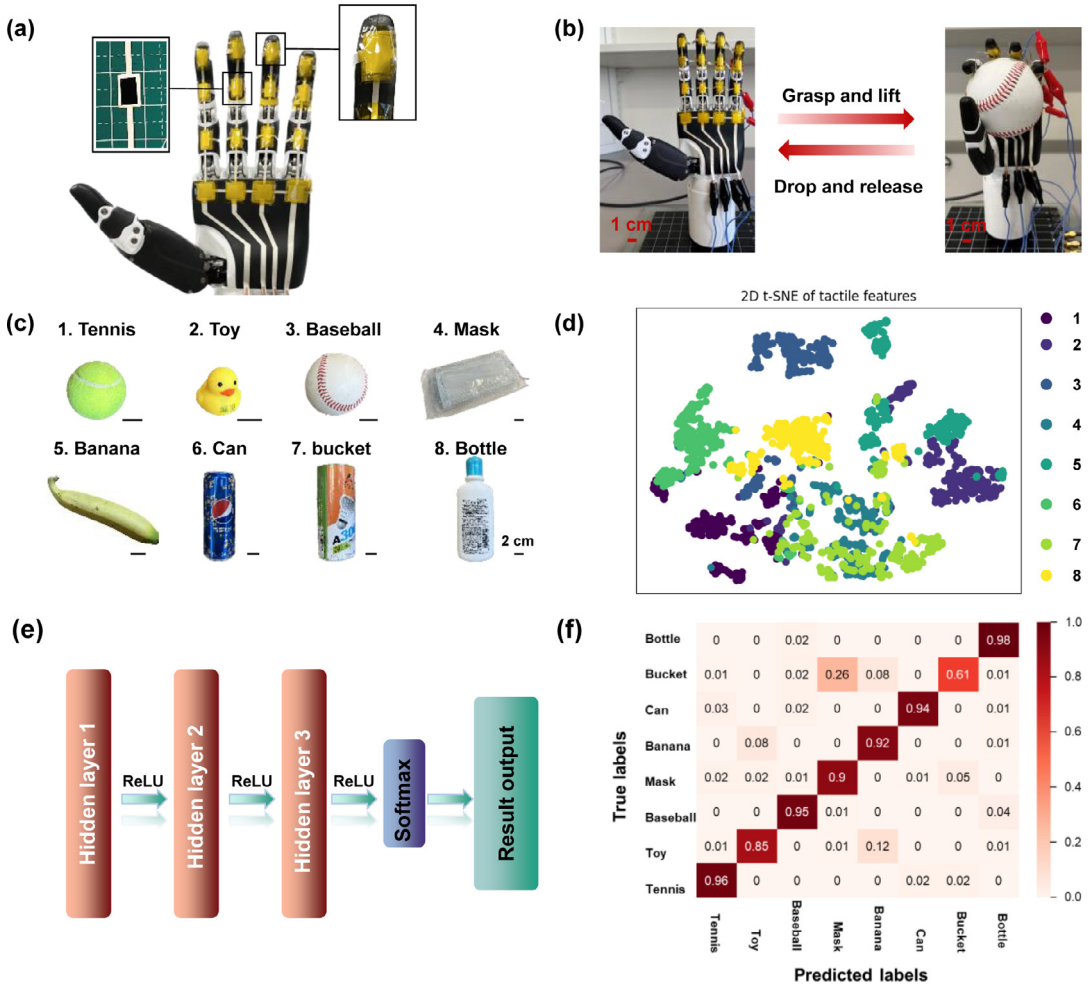

Fig. 5. Robotic hand integrated with 4 × 4 VG sensor array for sensing and object classification. (a) Schematic diagram of a robotic hand with an integrated 4 × 4 VG sensor array. The enlargement on the left shows an example of a VG electrode pre-adhered to the sensing area of a sensor array by a silver paste. (b) Optical photograph of a robotic hand grasping a baseball for tactile data acquisition with an integrated 4 × 4 VG sensor array. (c) Optical photos of eight different objects for intelligent robotic hand grasp recognition. (d) 2D visual projection of 2800 collected data using t-SNE. (e) Schematic diagram of the structure of the multilayer perceptron model to recognize objects with different shapes, sizes and materials. (f) Classification test confusion matrix for the test dataset (8 classes of objects, 840 samples); each row and column represent one instance in the predicted and true classes, respectively, and the diagonal values indicate the correct prediction results. The color bars indicate the accuracy of the prediction.

in Fig. 5a, we fix the 4 × 4 VG sensor array at the location where the robot hand has frequent contact with the object. The VG electrode with a branching flap shape is adhered to the sensing area of the pre-cut patterned electrode by means of a silver paste, as shown in the enlarged view on the left in the figure. The robotic hand used in the demonstration is purchased from Beijing Inspire Robotics Technology Co., Ltd. This robotic hand integrates six miniature servo cylinders, enabling object grasping through the motor-controlled bending of the robotic fingers. The operating voltage is set to 24 V. Fig. 5b records an optical photograph of the robotic hand grasping a baseball for real tactile information. We simultaneously record the signal of a frame of the tactile array after the grasp is stabilized. The whole grasping process is carried out by the experimenter giving the object to the manipulator. The direction and angle of the given object are randomly changed during the process to obtain more complete object grasping information. To minimize the impact of different grasping strengths and postures of the robotic hand on the grasping process, throughout the entire data collection process, we ensure that each grasp initiates finger bending movement at the same angle and speed through motor control. Additionally, when the robotic hand contacts the object and the gripping force reaches the set threshold, the grasping automatically stops and remains in that position. We operated the robotic hand to grasp eight objects of different shapes and materials at room temperature (Fig. 5c). Each of these objects is repeatedly grasped 350 times (2800 datasets in total) and alternated from different directions to ensure the accuracy of the robotic hand recognition system. The VG array response thermograms obtained from seven sets of randomly selected grips for each object are shown in Fig. S12 (online). As shown in Fig. 5d, the 2800 data collected are first projected visually using t-distributed stochastic neighbor embedding (t-SNE) for dimensionality reduction. Data for the same object are represented in the same color. It can be seen from the figure that the data of similar objects have some aggregation. This is due to the fact that the eight objects have different shapes and materials. This leads to differences in the response signals of each sensing unit in the VG sensor array after grasping by the robotic hand, which provides the possibility of object recognition. To demonstrate the effectiveness of the sensed data for perceptual categories, we used the classical MLP neural network and CNN to train the data, respectively. Fig. 5e illustrates the specific cognitive process of the MLP system. An MLP, containing three hidden layers, is built based on the Pytorch framework. We randomly selected 1960 data as the training set for training and optimizing the MLP model. The remaining 840 data are used as a test set to validate the trained model. Fig. 5f shows the classification test confusion matrix for the test dataset by comparing the predicted results with real objects. Where each row and column represent an instance in the predicted class and the real class, respectively. The diagonal values indicate the correct prediction results. Although there is a small amount of confusion in the identification of different classes, the total classification accuracy can reach 89.1%. The cognitive structure of the CNN is shown in Fig. S13 (online), and the total classification accuracy is very close to that of MLP, reaching 89.2%. Thanks to the excellent sensing performance of VG sensors, we can acquire high-quality signals with only 4 × 4 low-density arrays and achieve high accuracy without complex algorithms.

4. Discussion and conclusion

The use of VG electrodes with inclined flap-like branching microstructures reduces the effect of structural stiffening due to axial compression and effectively improves the compressibility of the sensors. The iontronic pressure sensor constructed with VG electrode can achieve an ultra-high sensitivity of 185.09 kPa^{-1}. And it can detect a small pressure of 0.49 Pa. At a high pressure of 10 kPa, the VG sensor exhibits a resolution of 25 Pa. The high sensitivity of the device over the entire applied pressure range results from the significant increase of the EDL capacitance caused by the compressive flexion of the VG flap-like branching structure. At the same time, this VG structure demonstrates excellent stability over 1000 compression/unloading cycles and bending/unloading cycles. We used the VG sensing array recognition system with MLP neural network to implement haptic cognitive functions in a manipulator. Through analysis of the response signals collected while the manipulator grasps objects of various materials and shapes, we can achieve recognition accuracy exceeding 89.1%. This underscores the significant potential for integrating haptic intelligence into manipulative systems.

Conflict of interest

The authors declare that they have no conflict of interest.

Acknowledgments

This work was supported by Guangdong Major Talent Project (2019CX01X014, and 2019QN01C177). We acknowledge the assistance of SUSTech Core Research Facilities.

Author contributions

Jing Yang and Taihong Wang conceived the idea and designed the experiments. Jing Yang conducted the majority of experiments. Zhibin Li built the sensor testing circuit. Ying Wu participated in sample fabrication. Yong Shen did the finite element analysis. Songhua Xiao, Jiansong Feng, Xu Zhang, and Yuwei Tang helped with the sensor and material characterizations. Sunan Ding and Xiaolong Chen contributed to the general discussion. The manuscript was written based on contributions of all authors.

Appendix A. Supplementary materials

Supplementary materials to this article can be found online at https://doi.org/10.1016/j.scib.2024.05.001.

References

[1] Sundaram S, Kellnhofer P, Li Y, et al. Learning the signatures of the human grasp using a scalable tactile glove. Nature 2019;569:698–702.
[2] Li G, Liu S, Wang L, et al. Skin-inspired quadruple tactile sensors integrated on a robot hand enable object recognition. Sci Robot 2020;5:eabc8134.
[3] Yu X, Xie Z, Yu Y, et al. Skin-integrated wireless haptic interfaces for virtual and augmented reality. Nature 2019;575:473–9.
[4] Yin J, Wang S, Di Carlo A, et al. Smart textiles for self-powered biomonitoring. Med-X 2023;1:3.
[5] Libanori A, Chen G, Zhao X, et al. Smart textiles for personalized healthcare. Nat Electron 2022;5:142–56.
[6] Zhou Y, Zhao X, Xu J, et al. Giant magnetoelastic effect in soft systems for bioelectronics. Nat Mater 2021;20:1670–6.
[7] Zhao X, Zhou Y, Xu J, et al. Soft fibers with magnetoelasticity for wearable electronics. Nat Commun 2021;12:6755.
[8] Bai N, Wang L, Xue Y, et al. Graded interlocks for iontronic pressure sensors with high sensitivity and high linearity over a broad range. ACS Nano 2022;16:4338–47.
[9] Mannsfeld SCB, Tee BCK, Stoltenberg RM, et al. Highly sensitive flexible pressure sensors with microstructured rubber dielectric layers. Nat Mater 2010;9:859–64.
[10] Lipomi DJ, Vosgueritchian M, Tee BCK, et al. Skin-like pressure and strain sensors based on transparent elastic films of carbon nanotubes. Nat Nanotechnol 2011;6:788–92.

[11] Amoli V, Kim JS, Jee E, et al. A bioinspired hydrogen bond-triggered ultrasensitive ionic mechanoreceptor skin. Nat Commun 2019;10:4019.
[12] Su Q, Zou Q, Li Y, et al. A stretchable and strain-unperturbed pressure sensor for motion interference–free tactile monitoring on skins. Sci Adv 2021;7:eabi4563.
[13] Shen Z, Zhu X, Majidi C, et al. Cutaneous ionogel mechanoreceptors for soft machines, physiological sensing, and amputee prostheses. Adv Mater 2021;33:2102069.
[14] Tao K, Chen Z, Yu J, et al. Ultra-sensitive, deformable, and transparent triboelectric tactile sensor based on micro-pyramid patterned ionic hydrogel for interactive human–machine interfaces. Adv Sci 2022;9:2104168.
[15] Kim JS, Lee SC, Hwang J, et al. Enhanced sensitivity of iontronic graphene tactile sensors facilitated by spreading of ionic liquid pinned on graphene grid. Adv Funct Mater 2020;30:1908993.
[16] Chang Y, Wang L, Li R, et al. First decade of interfacial iontronic sensing: From droplet sensors to artificial skins. Adv Mater 2021;33:2003464.
[17] Jin ML, Park S, Lee Y, et al. An ultrasensitive, visco-poroelastic artificial mechanotransducer skin inspired by Piezo2 protein in mammalian merkel cells. Adv Mater 2017;29:1605973.
[18] Luo Y, Chen X, Tian H, et al. Gecko-inspired slant hierarchical microstructure-based ultrasensitive iontronic pressure sensor for intelligent interaction. Research 2022;2022:9852138.
[19] Zhu P, Du H, Hou X, et al. Skin-electrode iontronic interface for mechanosensing. Nat Commun 2021;12:4731.
[20] Yang J, Li Z, Zhang X, et al. Merkel cell-like artificial mechanoreceptor with high sensitivity and high resolution over a wide linear range. Cell Rep Phys Sci 2022;3:101101.
[21] Kudin KN, Scuseria GE, Yakobson BI. C_2F, BN, and C nanoshell elasticity from *ab initio* computations. Phys Rev B 2001;64:235406.
[22] Sun J, Rattanasawatesun T, Tang P, et al. Insights into the mechanism for vertical graphene growth by plasma-enhanced chemical vapor deposition. ACS Appl Mater Interfaces 2022;14:7152–60.
[23] Wu Y. Effects of localized electric field on the growth of carbon nanowalls. Nano Lett 2002;2:355–9.
[24] Zhao J, Shaygan M, Eckert J, et al. A growth mechanism for free-standing vertical graphene. Nano Lett 2014;14:3064–71.
[25] Seo DH, Pineda S, Yick S, et al. Plasma-enabled sustainable elemental lifecycles: Honeycomb-derived graphenes for next-generation biosensors and supercapacitors. Green Chem 2015;17:2164–71.
[26] Niyogi S, Bekyarova E, Itkis ME, et al. Spectroscopy of covalently functionalized graphene. Nano Lett 2010;10:4061–6.
[27] Huang Z, Kong D, Zhang Y, et al. Vertical graphenes grown on a flexible graphite paper as an all-carbon current collector towards stable Li deposition. Research 2020;2020:7163948.
[28] Han ZJ, Pineda S, Murdock AT, et al. RuO_2-coated vertical graphene hybrid electrodes for high-performance solid-state supercapacitors. J Mater Chem A 2017;5:17293–301.
[29] Zheng W, Zhao X, Fu W. Review of vertical graphene and its applications. ACS Appl Mater Interfaces 2021;13:9561–79.
[30] Deng C, Gao P, Lan L, et al. Ultrasensitive and highly stretchable multifunctional strain sensors with timbre-recognition ability based on vertical graphene. Adv Funct Mater 2019;29:1907151.
[31] Zhao Y, Yang N, Chu X, et al. Wide-humidity range applicable, anti-freezing, and healable zwitterionic hydrogels for ion-leakage-free iontronic sensors. Adv Mater 2023;35:2211617.
[32] Lu P, Wang L, Zhu P, et al. Iontronic pressure sensor with high sensitivity and linear response over a wide pressure range based on soft micropillared electrodes. Sci Bull 2021;66:1091–100.
[33] Chen Q, Yang J, Chen B, et al. Wearable pressure sensors with capacitive response over a wide dynamic range. ACS Appl Mater Interfaces 2022;14:44642–51.

Jing Yang is a Ph.D. candidate at the Department of Electrical and Electronic Engineering, Southern University of Science and Technology (SUSTech). She received her B.S. and M.S. degrees from the College of Chemistry and Chemical Engineering, Hunan University and the Pen-Tung Sah Institute of Micro-Nano Science and Technology, Xiamen University, respectively. Her research interest focuses on the flexible electronic skins.

Zhibin Li is a Ph.D. candidate at the Department of Electrical and Electronic Engineering, SUSTech. He received his B.S. degree at the College of Logistics Engineering, Shanghai Maritime University. His research interest focuses on the flexible electronic skins.

Ying Wu is an associate research fellow at School of Integrated Circuits, Nanjing University (NJU). She received her Ph.D. degree from Condensed Matter Physics from University of Bath, United Kingdom at 2016. She did her postdoctoral research at University of Bath (2016–2018), Suzhou Institute of Nano-Tech and Nano-Bionics, Chinese Academy of Sciences (2018–2021) and Southern University of Science and Technology (2021–2023). Her research interest focuses on the mechanism and manipulation of interfacial physics and low-dimensional materials.

Sunan Ding is a distinguished professor at the School of Integrated Circuit, NJU. He received his Ph.D. degree from the Institute of Semiconductors, Chinese Academy of Sciences, in 1992. His research interest includes novel materials and advanced processes for IC applications, wide-band-gap semiconductor growth and devices, thin films, and surface/interface analysis.

Xiaolong Chen is an assistant professor at the Department of Electrical and Electronic Engineering, SUSTech. He received his Ph.D. degree from the Department of Physics, Hong Kong University of Science and Technology (HKUST). He served as a postdoctoral fellow at the University of Cambridge (2015–2016) and Yale University (2016–2018). His research interest focuses on the Optoelectronic devices.

Taihong Wang is a chair professor at the Department of Electrical and Electronic Engineering, SUSTech. He received his Ph.D. degree from the Chinese Academy of Sciences. His research interest focuses on Sensing and intelligent perception.